Clustering Phenomena of Implants in Tungsten Observed with THDS

Kolk, G.J. van der; Veen, A. van; Hosson, J.Th.M. de; Caspers, L.M.

Published in:
Nuclear Instruments & Methods in Physics Research Section B-Beam Interactions with Materials and Atoms

DOI:
10.1016/0168-583X(85)90011-4

Nuclear Instruments and Methods in Physics Research B6 (1985) 517–524
North-Holland, Amsterdam

CLUSTERING PHENOMENA OF IMPLANTS IN TUNGSTEN OBSERVED WITH THDS

G.J. van der KOLK [1]* A. van VEEN [1], J.Th.M. de HOSSON [2] and L.M. CASPERS [1]†

[1] *Delft University of Technology/Interuniversity Reactor Institute Delft, Mekelweg 15, 2629 JB Delft, The Netherlands*
[2] *University of Groningen, Materials Science Centre, Nijenborgh 18, 9747 AG Groningen, The Netherlands*

Received 23 July 1984

A W(100) single crystal was irradiated with 5–10 keV of different metallic species (Ag, Cu, Cr, Mn, Al and In). Subsequently the crystal was annealed at temperatures ranging from room temperature to 2400 K. Thermal helium desorption spectrometry (THDS) was applied to monitor the dissociation and clustering reactions of defect complexes either formed at room temperature during implantation or during partial annealing at a higher temperature. Strong evidence is found for clustering of Ag if implantation doses of Ag exceed 6×10^{12} Ag^+ cm^{-2}. For the implants Al, Cr, Cu and Mn, substantial clustering was not detected. For In, a conclusion could not be made concerning clustering since He does not bind to In in W at room temperature. Atomistic calculations are presented which indicate that clustering of the implants other than Ag would certainly be detected if the impurity atoms in the cluster all occupy lattice positions. Therefore we believe that thermally activated radiation enhanced diffusion is much more efficient for Ag than for Cu and Mn in W. For Cr and Al we cannot exclude enhanced diffusion, since the binding energies of Cr and Al to Cr- and Al-clusters in W, respectively, will be rather small. Of the implants Cu, Mn and Ag, the latter is the only one being oversized. A rather strong binding of vacancies to Ag is envisaged, which enables transport of the Ag atom, being part of a moving vacancy cluster.

1. Introduction

In studies in which ion implantation is used to obtain mixed surface layers, radiation enhanced diffusion plays an important role in determining the efficiency of the mixing process. Ion irradiation induced defect fluxes not only affect the efficiency of the process but also may lead to radiation induced segregation [1–3]. The latter phenomenon is made possible by the first. It may lead to undesirable effects like demixing of alloys or surface enrichment by one of the alloying components as a consequence of irradiation [4]. The temperature range where enhanced diffusion is favoured is an intermediate region in which vacancies are mobile and where the equilibrium concentration of vacancies is not very high. The excess vacancies present during the implantation may provide a transport mechanism for larger solutes. For smaller solutes in general an interstitial migration mechanism is assumed [1]. A phenomenon closely related to radiation enhanced diffusion is clustering. After 5 keV implantation of Kr into W and annealing to 1500 K clustering was observed with thermal helium desorption spectrometry (THDS) [5]. It was shown that the Kr atoms were transported along with the radiation produced vacancies.

In this study THDS is applied to study the initial phase of segregation of metallic implants on an atomic level. Essentially THDS is the decoration of defects with low energy implanted helium. The rapid interstitial diffusion of He through the crystal provides trapping of a fraction of the implanted He atoms at different defects. Due to different binding energies the various defects can be distinguished by monitoring the He release rate as a function of the temperature. Binding of He to substitutional impurities gives rise to unique desorption peaks, for a review see refs. [6–8]. The desorption temperature is shifted upwards if more impurity atoms are located close to each other on lattice positions. This provides a unique tool to study radiation induced segregation in the very early stage when only two or three solute atoms have clustered. The results presented in this paper are an extension of earlier published results on Kr-clustering [5] and Ag-clustering in W [9].

In section 2 the experimental results are presented, in section 3 static lattice calculations are presented which facilitate assignment of the different desorption peaks. In section 4 the defect assignments will be made and discussed.

2. Experimental results

2.1. Experimental

The experimental equipment has already been described in refs. [5] and [10]. The sample is the same

* Present address: Philips Research Laboratories, 5600 JA Eindhoven. The Netherlands.
† Sadly, Dr. L.M. Caspers died during the course of this work.

0168-583X/85/$03.30

W(100) single crystal used in earlier experiments. The sample is mounted in a large vacuum chamber on a rotatable platform such that the sample can face: a metal ion source (5–30 keV); a gas ion source (0.1–6 keV); and a quadrupole mass spectrometer. The gas ion beam (He beam) traverses a Wien filter. The high purity of the He gas used ensures that the fraction of impurity ions in the He beam is less than 10^{-4}. The metal ion beam is mass analysed by a magnetic separator ($M/\Delta M \sim 200$). Both beams are swept periodically (700 and 2500 Hz) by horizontal and vertical pairs of deflection plates to ensure a uniform distribution on the target. Computer controlled heating by electron bombardment on the rear of the target ensures linear heating with time during desorption or partial annealing. The temperature is obtained from a WRe3%–WRe25% thermocouple. The annealing scheme used in this study consisted of linear heating with time (heating rate $\beta = 40$ K/s) to a certain temperature followed by cooling. In general this leads to recovery steps at higher temperatures than seen with isochronal annealing procedures.

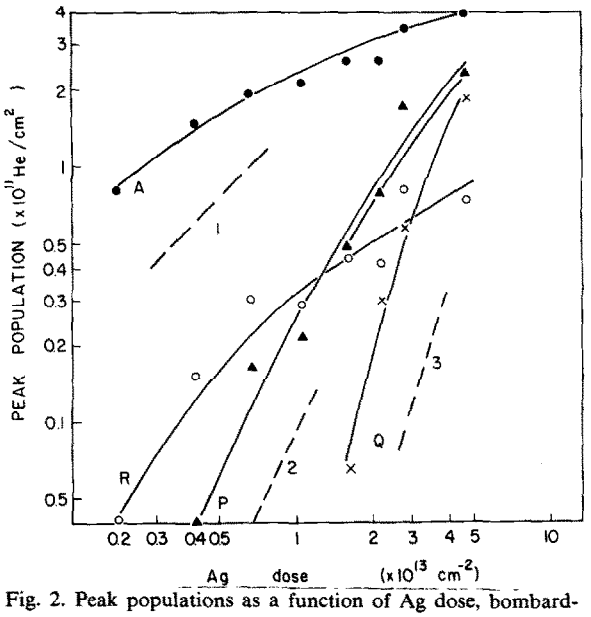

Fig. 2. Peak populations as a function of Ag dose, bombardment parameters as in fig. 1.

2.2. Results

2.2.1. Ag dose variation

In fig. 1 a series of desorption spectra is shown of W(100), implanted with an increasing dose of 10 keV Ag^+, heated to 1600 K and subsequently injected at room temperature with 1.3×10^{12} 250 eV He^+ cm^{-2}. The spectra are similar to those earlier shown [9], except for the appearance of a peak at low desorption tempera-

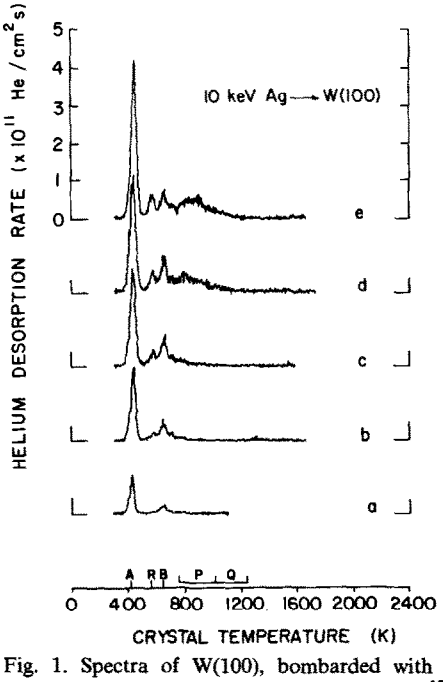

Fig. 1. Spectra of W(100), bombarded with 10 keV Ag^+, heated to 1600 K and injected with 1.2×10^{12} 250 eV He^+ cm^{-2}, Ag doses were: (a) 2×10^{12} cm^{-2}; (b) 4×10^{12} cm^{-2}; (c) 7×10^{12} cm^{-2}; (d) 2.1×10^{13} cm^{-2}; (e) 4×10^{13} cm^{-2}.

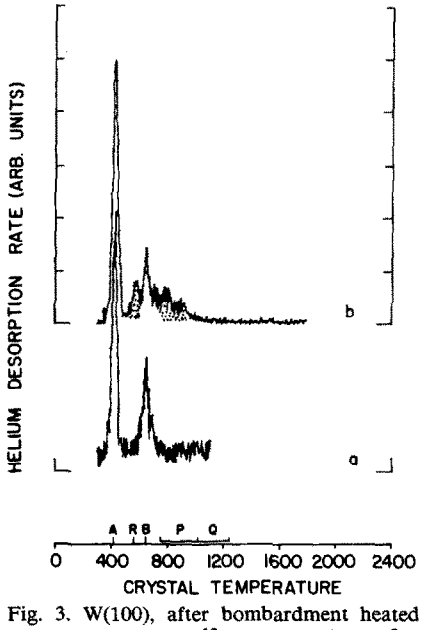

Fig. 3. W(100), after bombardment heated to 1600 K and injected with 1.3×10^{12} 250 eV He^+ cm^{-2}, shaded areas indicate high dose effects. Initial bombardments: (a) 1.7×10^{13} 20 keV W^+ cm^{-2}, followed by 1×10^{12} 10 keV Ag^+ cm^{-2} followed by 1.6×10^{13} 10 keV W^+ cm^{-2}; (b) 1.6×10^{13} 10 keV Ag^+ cm^{-2}.

Table 1
Peak assignments and dissociation parameters for Ag implanted W (heating rate 40 K/s)

Peak	Temp. (K)	E^d (eV)	ν_0 (s^{-1})	Reaction
A	430	1.03	3×10^{12}	$HeAgV \rightarrow He + AgV$
B	650	1.57	3×10^{12}	$He_2AgV \rightarrow 2He + AgV$
R	580	1.40	3×10^{12}	
P	760–1000	1.9–2.5	3×10^{12}	
Q	1000–1260	2.5–3.1	3×10^{12}	$HeAg_nV_n \rightarrow He + Ag_nV_n$ $n = 2,3$
H_b	1390	3.6	1×10^{13}	$HeAg_nV_{n+1} \rightarrow He + Ag_nV_{n+1}$
H	1490	4.5	2×10^{15}	$HeV \rightarrow He + V$

ture. A lower He dose is chosen than in ref. [9] to facilitate a better peak separation. The average degree of filling amounts to about 0.3 He per trap. In ref. [11] it was shown that the peaks labelled A and B represent dissociation of one or two He atoms respectively from a substitutional Ag atom (notation AgV). Extra peaks, labelled P, Q and R, are seen to evolve with increasing Ag dose. The P and Q peaks resemble the peaks seen earlier for high dose Kr bombardment on W [5], therefore the same notation was used. The different peaks, peak temperatures and dissociation energies for the indicated pre-exponential factors ν_0 are shown in table 1. It should be noted that the P and Q peaks are too broad to represent only one binding state; no proper fit could be made. Therefore all He desorbing between 760 K and 1000 K was taken as P peak population, and He desorbing above 1000 K but below 1200 K was taken as Q peak population. The peak assignments shown in the table will be discussed in the next section. The peak populations as a function of the Ag dose are shown in fig. 2.

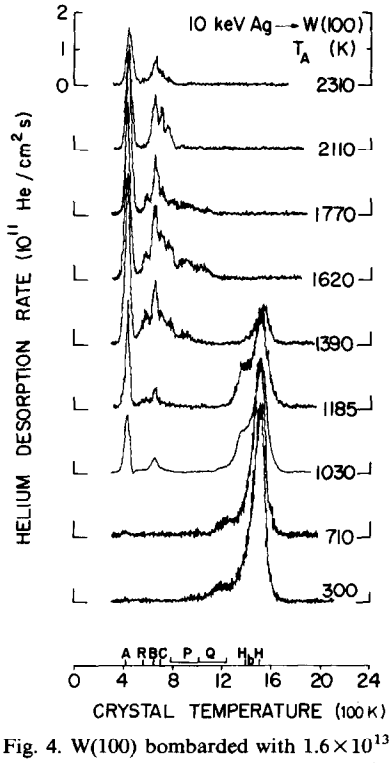

Fig. 4. W(100) bombarded with 1.6×10^{13} 10 keV Ag^+ cm^{-2}, heated to the indicated temperatures and injected with 3×10^{12} 250 eV He^+ cm^{-2}.

2.2.2. Influence of other defects

Implantation with 1.6×10^{13} 10 keV In^+ cm^{-2}, heating to 1600 K, and injection with 250 eV He^+ revealed no desorption peaks at all. From this we conclude that the P, Q and R peaks seen in the case of Ag implantation are associated with Ag. Location of Ag near implantation-produced defects may be responsible for the enhanced He binding. A Ag atom next to a dislocation loop will bind He stronger than a Ag atom in a perfect lattice. To investigate this the target was bombarded with a very high dose of 20 keV W^+ ions to create dislocation loops and vacancy clusters. Subsequently a low dose Ag^+ was injected followed by a bombardment with a high dose of W^+. Finally the crystal was heated to 1600 K. This "sandwich" bombardment ensures, wether the Ag atoms or the other defects are the mobile species, that the fraction of Ag

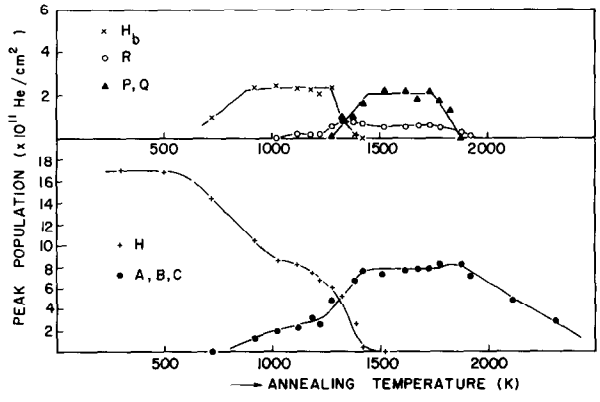

Fig. 5. Peak populations as a function of the annealing temperature, bombardment parameters as in fig. 4.

located near other defects will be of the same order of magnitude as in the case of high dose Ag bombardment only. The spectrum is shown in fig. 3. For comparison a spectrum with a high dose Ag only is also shown. It is quite clear that P, Q and R peaks are not visible in the case of pre- and post-irradiation with W ions.

2.2.3. Annealing behaviour of high dose Ag^+ implanted W

In fig. 4 a series of spectra is shown of W(100), bombarded with 1.6×10^{13} 10 keV Ag^+ cm^{-2}, annealed to the indicated temperatures and subsequently injected at room temperature with 3×10^{12} 250 eV He^+ cm^{-2}. The peak labelled H represents He desorption from vacancy type defects. Apparently the peak shown here after annealing to temperatures beyond stage III temperature (in our annealing scheme 900 K) originates from He trapped in bound vacancies since free vacancies do not survive this annealing temperature. The peak is labelled H_b. The vacancies can be bound to vacancy clusters or to Ag clusters. In fig. 5 peak populations as a function of the annealing temperature are shown. The following observations can be made:

1) After annealing to stage III (900 K) the H peak has decreased, monovacancies have become mobile and have disappeared at the near surface.
2) The A, B and C peaks become visible at about 90C K.
3) Above 700 K a peak denoted H_b becomes visible. The disappearance of peak H_b at 1350 K is accompanied with the appearance of the P and Q peaks.
4) Above 1800 K the P, Q and R peaks disappear in

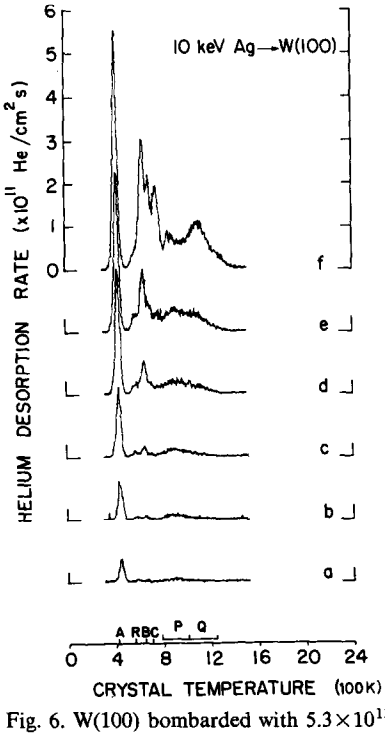

Fig. 6. W(100) bombarded with 5.3×10^{13} 10 keV Ag^+ cm^{-2}, heated to 1800 K and injected with various He doses, He doses were: (a) 2×10^{11} cm^{-2}; (b) 4.3×10^{11} cm^{-2}; (c) 8.6×10^{11} cm^{-2}; (d) 2×10^{12} cm^{-2}; (e) 3×10^{12} cm^{-2}; (f) 6×10^{12} cm^{-2}.

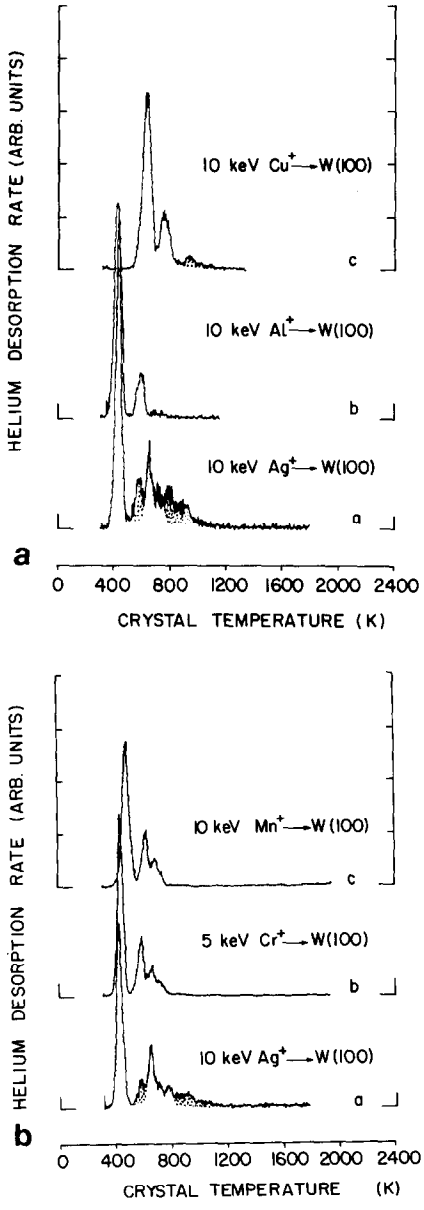

Fig. 7. (a) W(100) bombarded, heated to 1600 K and injected with 1.3×10^{12} 250 eV He^+ cm^{-2}, shaded areas indicate high dose effects. Initial bombardments: a) 1.6×10^{13} 10 keV Ag^+ cm^{-2}; b) 4×10^{13} 10 keV Al^+ cm^{-2}; c) 4×10^{13} 10 keV Cu^+ cm^{-2}. As (a) but with initial bombardments: a) 1.3×10^{13} 10 keV Ag^+ cm^{-2}; b) 2×10^{13} 5 keV Cr^+ cm^{-2}; c) 2.6×10^{13} 10 keV Mn^+ cm^{-2}.

Table 2
Calculated dissociation energies E^d for He from various defects. Figures between brackets indicate nth neighbour positions.

Defect	E^d (eV) calc.	E^d (eV) exp.
AgV	1.00	1.03
$Ag_2V_2(1)$	1.58	
$Ag_2V_2(2)$	1.72	
$Ag_3V_3(112)$	2.29	
CuV	1.76	1.48
$Cu_2V_2(1)$	2.26	
$Cu_2V_2(2)$	2.97	
MnV	1.17	1.13
$Mn_2V_2(1)$	1.31	
$Mn_2V_2(2)$	2.11	
CrV	1.25	1.02
$Cr_2V_2(1)$	1.33	
$Cr_2V_2(2)$	2.09	
AlV	1.21	0.99
$Al_2V_2(1)$	1.48	
$Al_2V_2(2)$	1.99	

narrow temperature interval.

5) Above 1800 K the A, B and C peaks gradually disappear apparently due to thermal vacancy assisted diffusion of the Ag atoms to the surface followed by desorption [11,12].

2.2.4. He dose variation after high dose Ag^+ implantation

The He dose was varied for the W target implanted with 5.3×10^{13} 10 keV Ag^+ cm^{-2} and annealed to 1800 K. The spectra are shown in fig. 6. It is quite clear that the average desorption temperature of the peaks, evolving after high dose Ag implantation, increases with increasing He dose.

2.2.5. High doses of Cu^+, Al^+, Mn^+, Cr^+ and In^+

In fig. 7 spectra, taken after high dose impurity bombardment and annealing to 1600 K, are shown for the various other implants. Spectra for In implantation are not shown, since In in W does not bind He at all. Quite evidently the characteristic P, Q and R peaks are not visible for the implants other than Ag. However in the case of Cu^+ implantation a very small peak is visible at 950 K which should not be there at the low He filling degree of the defects.

3. Static lattice calculations

Static lattice calculations were performed for various impurity clusters to obtain an estimate of the binding energies of He. The pair-potential set was the same as used in [11]. The W–W potential was derived from elastic constants [13], the He–metal pair potentials were derived with a Hartree–Fock–Slater scheme [14,15]. The W–impurity and impurity–impurity potentials were obtained by application of a scaling procedure to the W–W potentials [11]. The size of the crystallite in the calculations is $17 \times 17 \times 17$ lattice units.

From the calculations binding energies were obtained. The dissociation energy equals the binding plus migration energy, therefore 0.25 eV was added to all calculated binding energies to obtain the dissociation energies. In table 2 results are shown for the substitutional implants as well as for the small clusters. The number between brackets indicates a substitutional impurity at nth neighbour separation. The configuration of a diatomic impurity cluster which yielded the largest He dissociation energy was the second nearest neighbour cluster. Impurity atoms at nth neighbour distance with $n > 2$ affect the binding energies only slightly. For the triatomic clusters surrounding of the He atom leads to the highest binding energy. To illustrate the accuracy of the calculations, we show in table 2 the experimental dissociation energies for He from substitutional implants taken from [11].

4. Discussion

4.1. Ag results

The P, Q and R peaks were seen to evolve at higher Ag doses only. For the other implants no P and Q peaks were seen. Since for high dose In implantation He binding was not observed at all, whereas the cascades produced by In and Ag are similar, we believe that the P and Q peaks have to do with He associated with Ag (similarly as for Kr). Other evidence is that after Kr bombardment a P peak was observed at a higher desorption temperature than for Ag for a similar He dose [5]. There are various arguments which support the assignment of these peaks to Ag clusters as well as undermining this assignment. The following arguments undermine the clustering hypothesis:

(1) After implantation of a W foil with 25 keV $^{111}Ag^+$ to a dose of 2×10^{13} cm^{-2} and isochronal annealing at 1200 K, observations with perturbed angular correlation measurements (PAC) did not reveal sizable contributions to the PAC spectra with hyperfine parameters as would be expected for diatomic Ag clusters [16].

(2) Only the R peak is a clear first order desorption peak, the P and Q peaks are in fact conglomerates of (probably first order) desorption peaks with slightly different desorption temperatures.

Arguments which support the clustering hypothesis are:

(1) No P, Q and R peaks could be grown in the W target by bombardment with a high dose 20 keV W^+, followed by a low dose 10 keV Ag^+ and again bombarded with a high dose 10 keV W^+.

(2) In the case of 10 keV Ag^+ bombardment, conversion of vacancy type peaks into P and Q peaks takes place at a considerably lower annealing temperature than in the case of 5 keV Kr^+ bombardment. The higher implantation energy of Ag will lead to larger defect clusters, so the weaker vacancy binding is caused by a weaker interaction of the vacancies with the implanted atoms, i.e. Ag-atoms. The strong vacancy binding observed in both cases is not expected for single substitutional impurities.

(3) The P, Q and R peaks are seen already at an implantation energy of 5 keV, this implantation energy is too low to expect large defect clusters to have formed. Small defect clusters other than Ag-clusters may have formed, but we do not expect that these are stable up to 1800 K.

(4) The peak evolution of the P, Q and R peaks is for the P and R peaks approximately quadratic with the Ag dose, whereas for the Q complex a higher order increase is seen as a function of the Ag dose (see fig. 2). Especially the latter observation supports the clustering hypothesis since it is hard to see why a third order term would persist for Ag interaction with other defects as a function of the bombardment dose.

A unique assignment of the P, Q and R peaks is not possible. Based on the above arguments, however, we believe that the P and Q peaks represent binding of He to small Ag clusters. The R peak will not necessarily indicate clustering; it only grows quadratically with Ag dose for low doses, at higher doses a saturation occurs (see fig. 2). Maybe Ag clusters in near surface regions give rise to this peak. It should be noted that for Kr the R peak was not observed [5]. Since the He filling degree in these experiments was rather high, it cannot be excluded that the R peak was hidden underneath the B and C peaks.

The calculated binding energies also do not permit a definite assignment of the P, Q and R peaks. The computed dissociation energy of He to, what is expected to be the most stable diatomic Ag-cluster, a $Ag_2V_2(1)$, is well in between the two experimental values of the R and P peaks. All experimental values however are well in the range of what is computed for small Ag-clusters.

Assuming that the P and Q peaks represent clustering the annealing results are explained as follows: vacancy type defects are visible up to 1400 K, however the largest fraction has disappeared after annealing to 1100 K. The fraction still visible will be due to bound vacancies and to more stable vacancy clusters. At 1300 K the peak labelled H_b disappears accompanied with a growth of the P and Q peaks. Since the maximum peak temperature of H_b is lower than that of the pure H peak after low dose implantation, we believe that dissociation of He from vacancy type defects slightly "smaller" than monovacancies is concerned here. Ag is oversized in W, so a vacancy bound by a Ag-cluster will indeed be "smaller'. Note that in ref. [16] a binding energy of a vacancy to a substitutional Ag-atom in W was found of 0.5 eV. For two atoms a binding energy approximately two time larger is expected. This would result in a dissociation energy of 2.7 eV. The recovery step at 1300 K corresponds with about 3.5 eV. In the earlier Kr clustering experiments vacancy type defects persisted up to much higher annealing temperatures. This is quite understandable regarding the much larger binding energy of a vacancy to a KrV than to a AgV in tungsten. A Kr_2V_3 will similarly be more stable than a Ag_2V_3.

The P, Q and R peaks disappear at about 1800 K. This corresponds with the onset of self-diffusion via a thermal vacancy mechanism. So the Ag clusters break up, essentially this requires only one step versus many for migration to the surface. Indeed it is observed that the decrease of the P, Q and R peaks is rather sudden.

4.2. Other metallic implants

The small peak visible after high dose Cu injection at 950 K in fig. 6 (corresponding for $\nu_0 = 3 \times 10^{12}\ s^{-1}$ with $E^d = 2.3$ eV) agrees with the dissocation energy of 2.26 eV, calculated for He dissociation from a Cu_2V_2. Therefore we assume that this peak indicates Cu clustering. For the other implants, Cr, Al and Mn, no clustering peaks were observed. We cannot exclude, however, that a peak of the same magnitude of the cluster peak in the case of Cu is hidden underneath the B and C peak. The calculations predict an enhancement of the binding energy of only 0.1–0.3 eV for the smallest clusters. Quite evidently for all these implants the degree of clustering is far below that of Ag in W.

4.3. Mobility and clustering mechanism

According to Miedema et al. [17] Ag, Cu and Mn have a positive heat of solution in liquid W. The binding energy between two solute atoms is proportional to the reduction of the contact area implant–host. Neglecting contributions due to size-mismatch and taking the reduction 1/8 for a diatomic cluster with respect to two isolated atoms, the following data were obtained for the binding energy: for Ag 0.21 eV, for Cu 0.11 eV and for Mn 0.03 eV.

Transport of the solute atoms can occur through two mechanisms:

(1) The substitutional implants are converted to interstitial positions by interaction with irradiation produced self-interstitials [18]. Once in interstitial position diffusion may occur quite easily. A large fraction of these interstitials however, will be trapped by nearby

vacancies of their own cascade. Those interstitials escaping their cascade, will still have a rather small probability of encountering another implant, since these are effectively shielded by vacancies as well.

(2) The substitutional implants bind one or more vacancies, the whole complex migrates thermally activated.

Since the appearance of the P and Q peaks coincides with the disappearance of the vacancy-type peak H_b, we assume that indeed the latter mechanism is responsible for the observed clustering. The first mechanism may play an additional role in the transportation of impurity atoms to the cascade regions of other implanted atoms.

The binding energy of a vacancy to Ag in W was recently measured; and is 0.5 eV [16]. Adopting "Miedema type" arguments we expect that the vacancy binding energy is related to the positive heat of solution and the relative oversize of the impurity atom [19]. After correction for volume contraction due to charge transfer, similarly as in ref. [11], Ag is the only oversized implant of the impurities studied here. Furthermore it has the highest heat of solution. Therefore we expect that the vacancy binding energy to the other impurities is well below the experimental value found for Ag. Consequently, the mobility of the other implants will be smaller than that of Ag.

Observing fig. 7 we notice that already at Ag doses of 6×10^{12} Ag^+ cm^{-2} clustering is visible. From the model given by van Gorkum et al. [20] it is deduced that the probability p_c that an implanted atom encounters another implanted atom, is approximately:

$$p_c = 4\pi r_i \bar{d}_i c_i f_m. \quad (1)$$

r_i is the trapping radius for implants, for noble gas atoms r_i is typically 3 Å, $\bar{d}_i$ is the average penetration depth of the implant, c_i the concentration per surface area and f_m a factor which indicates the fraction of the implants which is sufficiently long associated with a vacancy to facilitate long range transport. A rough guess of the latter follows from the desorption data of Kornelsen et al. [21] of 5 keV Kr implanted into W(100). Only some 10% of the Kr atoms has desorbed from the crystal after heating to 1600 K (heating rate 40 K/s). A large fraction is due to desorption of near-surface Kr. An upper limit of f_m for implantation energies of about 5 keV will therefore be 0.05.

Average penetration depths calculated with Marlowe of 10 keV Ag implanted into W(100) at implantation angles of 10° respectively 20° off the surface normal are respectively 125 Å and 30 Å. Therefore we expect from eq. (1) that for a Ag dose of 1×10^{13} cm^{-2} a fraction of between 6% and 24% has clustered. Indeed for a Ag dose of 1×10^{13} cm^{-2} 10% of the trapped He atoms desorbs in the P and Q peaks.

5. Conclusions

(1) After bombardment with doses above 6×10^{12} 10 keV Ag^+ cm^{-2} and annealing to 1200 K extra peaks were seen in the desorption spectra, which were attributed to He desorbing from small Ag_nV_n clusters, with $n = 2,3, \cdots$. The peaks disappeared after annealing to 1800 K, the decrease is rather abrupt, indicating that only one step is needed for the cluster to break up. The appearance of the cluster peaks is accompanied with the disappearance of a vacancy type peak H_b. He desorbing from a vacancy, bound by a small Ag cluster, causes this peak. It indicates that the Ag clusters form through excess vacancies.

(2) The P and Q peaks are too broad for first order desorption peaks. This could be caused by a variety of defects with slightly different binding energies for He, such as location of the clusters near other defects, near the surface, or various cluster configurations.

(3) For the other implants Cu, Mn, Al and Cr no substantial clustering was observed. Both the binding energy between these implants and a vacancy and the mutual binding energy are lower than for Ag. The first will hamper the impurity transport, the second will lead to a lower clustered fraction for similar mobilities as for Ag.

Although thermal activation was needed in this study to obtain clustering, we believe, that the findings in this study strongly support the model that radiation enhanced diffusion and radiation induced segregation for oversized solutes takes place through a bound vacancy–solute complex.

This work was partly financed by the Stichting voor Fundamenteel Onderzoek der Materie (Foundation for Fundamental Research on Matter) subsidized through the Nederlandse Organisatie voor Zuiver Wetenschappelijk Onderzoek (Netherlands Organization for the Advancement of Pure Research).

References

[1] A.D. Marwick, Nucl. Instr. and Meth. 182/183 (1981) 827.
[2] A.D. Marwick and R.C. Piller, Nucl. Instr. and Meth. 182/183 (1981) 121.
[3] G. Martin, R. Cauvin, J.-L. Bocquet and A. Barbu, in Point defects and defect interactions in metals, eds., J. Takamura, M. Doyama and M. Kiritani (North-Holland, Amsterdam, 1982) pp. 923–930.
[4] L.E. Rehn, in Metastable materials formation by ion implantation, eds., S.T. Picreaux and W.J. Choyke (North-Holland, Amsterdam, 1982) pp. 17–34.
[5] A. van Veen, A. Warnaar and L.M. Caspers, Vacuum 30 (1980) 109.
[6] E.V. Kornelsen, Rad. Eff. 13 (1972) 227.

[7] L.M. Caspers and A. van Veen, Phys. Stat. Sol. (a) 68 (1981) 339.
[8] E.V. Kornelsen and A.A. van Gorkum, Vacuum 31 (1981) 99.
[9] G.J. van der Kolk, A.S. Hydra, A. van Veen and L.M. Caspers, Nucl. Instr. and Meth. 209/210 (1983) 1047.
[10] G.J. van der Kolk, A. van Veen, L.M. Caspers and J.Th.M. de Hosson, Rad. Eff. 71 (1983) 109.
[11] G.J. van der Kolk, A. van Veen, L.M. Caspers and J.Th.M. de Hosson, accepted by J. Nucl. Mater.
[12] M. Paunov and E. Michailov, Surface Sci. 81 (1979) 479.
[13] R.A. Johnson and W.D. Wilson, in Interatomic potentials and simulation of lattice defects, eds., P.C. Gehlen, J.R. Beeler Jr. and R.I. Jaffee (Plenum, New York, 1972) p. 301.
[14] P.T. Wedepohl, Proc. Phys. Soc. 92 (1967) 79.
[15] W.D. Wilson and C.L. Bisson, Phys. Rev. B 3 (1971) 3984.
[16] G.J. van der Kolk, K. Post, A. van Veen, F. Pleiter and J.Th.M. de Hosson, accepted by Rad. Eff.
[17] A.R. Miedema, F.R. de Boer and R. Boom, Calphad 1 (1977) 341.
[18] G.J. van der Kolk, A. van Veen, L.M. Caspers and J.Th.M. de Hosson, accepted by Rad. Eff. Lett.
[19] A.R. Miedema, Z. Metallkunde 70 (1979) 345.
[20] A.A. van Gorkum and E.V. Kornelsen, Rad. Eff. 42 (1979) 93.
[21] E.V. Kornelsen and M.K. Sinha, J. Appl. Phys. 39 (1968) 4546.